Memristive Rulkov Neuron Model With Magnetic Induction Effects

Kexin Li , Han Bao , Houzhen Li , *Graduate Student Member, IEEE*, Jun Ma ,
Zhongyun Hua , *Member, IEEE*, and Bocheng Bao , *Member, IEEE*

Abstract—The magnetic induction effects have been emulated by various continuous memristive models but they have not been successfully described by a discrete memristive model yet. To address this issue, this article first constructs a discrete memristor and then presents a discrete memristive Rulkov (m-Rulkov) neuron model. The bifurcation routes of the m-Rulkov model are declared by detecting the eigenvalue loci. Using numerical measures, we investigate the complex dynamics shown in the m-Rulkov model, including regime transition behaviors, transient chaotic bursting regimes, and hyperchaotic firing behaviors, all of which are closely relied on the memristor parameter. Consequently, the involvement of memristor can be used to simulate the magnetic induction effects in such a discrete neuron model. Besides, we elaborate a hardware platform for implementing the m-Rulkov model and acquire diverse spiking-bursting sequences. These results show that the presented model is viable to better characterize the actual firing activities in biological neurons than the Rulkov model when biophysical memory effect is supplied.

Index Terms—Initial state, magnetic induction, memristive rulkov (m-Rulkov) model, regime transition, transient chaos.

I. INTRODUCTION

AS WITH conventional chaotic systems, a nervous system also involves various nonlinearities. The nonlinearity in nervous systems plays a vital role in generating spiking-bursting regimes and chaotic dynamics [1]. However, all these nonlinearities seldom contain internal variables with physical effects. A memristor is a nonlinear circuit element whose physical attributes make it have special nonlinearities with internal

Kexin Li, Han Bao, Houzhen Li, and Bocheng Bao are with the School of Microelectronics and Control Engineering, Changzhou University, Changzhou 213164, China (e-mail: likexincczu@163.com; charlesbao0319@gmail.com; leehzh@126.com; mervinbao@126.com).

Jun Ma is with the Department of Physics, Lanzhou University of Technology, Lanzhou 730050, China (e-mail: hyperchaos@163.com).

Zhongyun Hua is with the School of Computer Science and Technology, Harbin Institute of Technology, Shenzhen 518055, China (e-mail: huazyum@gmail.com).

variables (electric charge or magnetic flux) [2]. Thus, there is an essential difference between memristive nonlinearity and conventional nonlinearity [3], [4]. Thanks to the distinctive nonlinearities, the memristors have been broadly applied in chaotic systems and neural circuits [4]–[6].

The memristors can be used to simulate neural synapses or to characterize magnetic induction [5] when extracellular and intracellular ions are propagated in the cell. Most of the previous mathematical and biological neuron models have been built to show the main dynamical properties and firing patterns that are similar to the experimental series for membrane potentials from biological cells and tissue, while the potential physical field effect has not been explored, yet. That is, the involvement of memristors into neural circuits can reliably estimate the biophysical effect when neural activities are triggered. The Hodgkin–Huxley model [7] and Morris–Lecar model [8] were built on the basis of the ion-channels of neurons, and their stochastic ion-channels can be tamed as memristors [9], [10] and ions propagation can be controlled completely. Yao *et al.* [11] reported that the fully hardware-implemented memristor neuromorphic system provides an energy-efficient approach to training neural networks. Kumar *et al.* [12] demonstrated that the efficiency and accuracy of Hopfield computing network to converge to a solution are both greatly enhanced when being incorporated with memristors. Sangwan *et al.* [13] developed a hybrid memristor transistor and showed the gate tunability, large switching ratios, and long-term retention of states. Fu *et al.* [14] exhibited a type of diffusive memristors and their ability to process biosensing signals. Kumar *et al.* [15] verified that a third-order memristor element exhibits chaotic dynamics and thus enables densely functional neuromorphic computing primitives. Hong *et al.* [16] proposed a self-repairing astrocyte-neuron network using memristors to imitate changes in neurotransmitters. Furthermore, when embodying memristors, the performance of the cellular neural network was further enhanced and the speed for pattern recognition and image processing was thereby raised [17]. By imitating the short-term facilitation and long-term potentiation, the neurochemical foundations for learning and memory were demonstrated in a memristor-based neural circuit [18]. In summary, the memristors have attracted considerable attention from researchers and increasingly become the crucial components of neuromorphic circuits.

The occurrence of action potential in neurons can induce a magnetic induction flow [19]. When the neuron firing activities are related with the magnetic induction, a memristor-enabled

neuron model can be employed for characterizing the magnetic induction effect [5], [20]. Using this scheme, many memristor coupled neuron models were built and numerous complex firing behaviors were revealed [21]–[23]. So far, however, this scheme was applied only to continuous memristor neuron models. How to apply this scheme in discrete memristor neuron models is still a challenging problem. Hence, introducing a memristor into a discrete neuron model and finding out its dynamical effect on the spiking-bursting behaviors are difficult but attractive research works. Recently, a discrete memristor was proposed by discretizing a continuous memristor [24]. Meanwhile, several examples of discrete memristive maps were provided by coupling a discrete memristor with some existing discrete maps [25]. Inspired by this beneficial idea, this article first constructs a new discrete memristor with hyperbolic tangent memductance from a continuous memristor in [5] and then couples the discrete memristor with the 2-D Rulkov model [26] to establish a memristive Rulkov (m-Rulkov) neuron model with a specially imposed influence. Particularly, the m-Rulkov model can commendably manifest the memristor-simulated magnetic induction effect and memristor initial state-relied extreme multistability [27].

The main contributions and novelty of this study are summarized as follows.

1) We construct a discrete memristor and present an m-Rulkov neuron model. To the best of our knowledge, this is the first time that a discrete memristor-based neuron model is presented.

2) To show the complex dynamics in the m-Rulkov model, we investigate the magnetic induction-related regime transition behaviors, transient chaotic bursting regimes, and hyperchaotic firing behaviors. The memristor initial state-relied bifurcation behaviors manifest that the m-Rulkov model exhibits the striking phenomenon of extreme multistability.

3) A hardware platform for implementing the m-Rulkov model is elaborated and diverse spiking-bursting sequences are acquired in physical. Compared with continuous neuron models, the presented discrete neuron model has lower dimensions for generating hyperchaotic behaviors and can produce random numbers with higher randomness.

The rest of this article is organized as follows. Section II constructs a discrete memristor and presents an m-Rulkov model. Section III investigates the magnetic induction-related regime transition behaviors and transient chaotic bursting regimes. Section IV studies the memristor-related hyperchaotic firing behaviors. Section V elaborates a hardware platform to acquire diverse spiking-bursting sequences. Finally, Section VI concludes this article.

II. PRESENTED M-RULKOV NEURON MODEL

This section first constructs a new discrete memristor and inspects its frequency/initial state-relied voltage-current loci. Afterwards, this section presents an m-Rulkov neuron model while considering the magnetic induction.

A. Discrete Memristor and Its Fingerprints

Memeristor can be used to simulate the magnetic induction of neuron action potential. If a neuron is described by a discrete model, e.g., the 2-D Rulkov model [26], its involved memristor simulating the magnetic induction should also be discretized.

A flux-controlled memristor was presented to simulate the magnetic induction recently [5]. It can be remodeled as follows:

$$i = W(\varphi)v = \tanh(\varphi)v, \, \mathrm{d}\varphi/\mathrm{d}\tau = v \qquad (1)$$

where φ is the flux variable, τ is the time variable, and v and i are the voltage and current of the memristor. The memductance $W(\varphi) = \tanh(\varphi)$ shows that the memristor with the hyperbolic tangent memductance is smooth, nonlinear, and bounded. Therefore, the memristor has a distinctive nonlinearity due to its internal variable φ [3], and its nonlinearity is completely different from the conventional nonlinearity.

Following the continuous memristor discretization method in [24] and [25], we can obtain a discrete model for the memristor described in (1). Let v_n, i_n, and φ_n be the values of $v(t)$, $i(t)$, and $\varphi(t)$ at the n-th iteration, respectively. Then, the discrete model of the memristor can be built by

$$i_n = W(\varphi_n)v_n = \tanh(\varphi_n)v_n,$$
$$\varphi_{n+1} = \varphi_n + \varepsilon v_n \qquad (2)$$

where φ_{n+1} is the value of $\varphi(t)$ at the $(n+1)$th iteration. The parameter ε represents the scale factor of time for generating the induced electromotive force within finite transient period depended on the property of the media. To study the magnetic induction effects of the memristor on the neuron model, ε is set to 1 and 0.05 as two special examples, in which the larger value is used to generate hyperchaos while the smaller value is used to generate bursting firings.

The hyperbolic tangent memductance given in (2) is a single-valued function, whereas the cosine memductance or cosine memristance in [24] and [25] is a multivalued function. On the other hand, high nonlinearity in the memductance indicates rapid switch and thus discrete relation for $v-i$ is more suitable to estimate the transient activation and memory effect is reproduced completely. From the biological viewpoint, ions and charges are pumped suddenly when the channel is activated and then the ions propagation becomes stable. Therefore, a discrete modeling approach is more appropriate to estimate the ions pumping and action potential along the synapse than a continuous modeling approach.

To show the voltage–current loci of the discrete memristor given in (2), we add a discrete voltage $v_n = H \sin(\omega n)$ to the input of the discrete memristor [25]. Here, H and ω are the amplitude and angular frequency of the discrete voltage. First, let $\varepsilon = 1$. For $\omega = 0.1, 0.2, 0.4$, and 0.8 with $H = 0.1$ and $\varphi_0 = -0.1$, the frequency-relied voltage-current loci in the $v_n - i_n$ plane are plotted in Fig. 1(a). Meanwhile, for $\varphi_0 = -1, -0.5, -0.1$, and 0.5 with fixed $H = 0.1$ and $\omega = 0.2$, the initial state-relied voltage-current loci in the $v_n - i_n$ plane are plotted in Fig. 1(b). Second, denote $\varepsilon = 0.05$. For $\omega = 0.05, 0.1, 0.2$, and 0.4 with $H = 1$ and $\varphi_0 = 0$, the frequency-relied voltage–current loci in the $v_n - i_n$ plane are drawn in Fig. 2(a). And for $\varphi_0 =$
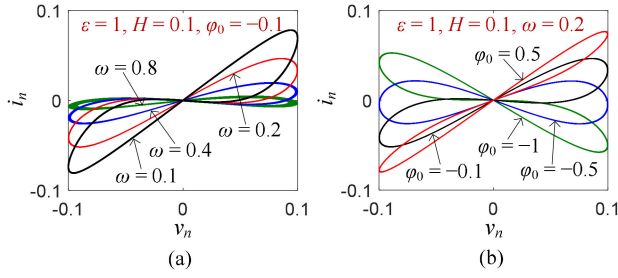
Fig. 1. For $\varepsilon = 1$, the fingerprints of the discrete memristor driven by $v_n = H\sin(\omega n)$. (a) Frequency-relied voltage-current loci for $\omega = 0.1$, 0.2, 0.4, and 0.8 with $H = 0.1$ and $\varphi_0 = -0.1$. (b) Initial state-relied voltage-current loci for $\varphi_0 = -1, -0.5, -0.1$, and 0.5 with fixed $H = 0.1$ and $\omega = 0.2$.
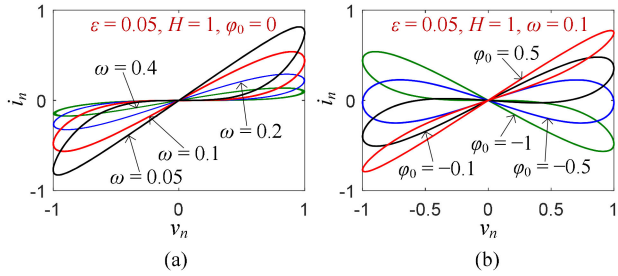

Fig. 2. For $\varepsilon = 0.05$, the fingerprints of the discrete memristor driven by $v_n = H\sin(\omega n)$. (a) Frequency-relied voltage-current loci for $\omega = 0.05, 0.1, 0.2$, and 0.4 with $H = 1$ and $\varphi_0 = 0$ (b) Initial state-relied voltage-current loci for $\varphi_0 = -1, -0.5, -0.1$, and 0.5 with fixed $H = 1$ and $\omega = 0.1$.

$-1, -0.5, -0.1$, and 0.5 with fixed $H = 1$ and $\omega = 0.1$, the initial state-relied voltage-current loci in the $v_n - i_n$ plane are drawn in Fig. 2(b). As can be observed, the voltage–current loci in Figs. 1 and 2 perfectly illustrate the fingerprints of the discrete memristor, similar to those of the continuous memristor.

More importantly, the initial state-relied voltage-current loci can show the special memory effect of the discrete memristor. As the initial state changes, the local activity of the discrete memristor also changes, which will affect the firing behaviors of a discrete neuron model when the memristor is incorporated. Thus, a discrete memristor is constructed to simulate the magnetic induction induced by the action potential in the discrete neuron model.

B. Discrete m-Rulkov Neuron Model

Most continuous neuron model, such as Hodgkin–Huxley model [7], Morris–Lecar model [8], and leaky integrate-and-fire model [28], were based on biophysical assumptions. However, the discrete Rulkov model with simple algebraic structure was built on dynamical assumptions. It is a 2-D discrete map that replicates neuronal firing activities [26], [29]. Relatively speaking, the discrete model is more suitable for digital circuit implementation than the continuous model [30]. When the firing activities are produced by a neuron, the Rulkov model can be written as follows:

$$\begin{cases} x_{n+1} = F(x_n, y_n), \\ y_{n+1} = y_n - \mu(x_n - \sigma + 1) \end{cases} \tag{3}$$

where x_n is the excitatory variable representing the action potential, y_n is the recovery variable, μ is the control parameter, and σ is the externally imposed influence. The $F(x, y)$ is a nonlinear and discontinuous function and can be described as follows:

$$F(x, y) = \begin{cases} \alpha/(1-x) + y, x \leq 0, \\ \alpha + y, 0 < x < \alpha + y, \\ -1, x \geq \alpha + y \end{cases} \tag{4}$$

where α is the control parameter.

Similar to the continuous neuron with memristive magnetic induction reported in [5], the memristive magnetic induction induced by stochastic pumping of ions and action potential can be also taken into account for a discrete neuron. Thus, a discrete m-Rulkov model with magnetic induction is obtained by the following:

$$\begin{cases} x_{n+1} = F(x_n, y_n) + k\tanh(\varphi_n)x_n, \\ y_{n+1} = y_n - \mu x_n, \\ \varphi_{n+1} = \varphi_n + \varepsilon x_n \end{cases}. \tag{5}$$

The additive term $k\tanh(\varphi_n)x_n$ indicates the magnetic induction current with an induction strength k, which is induced by the action potential x_n in (3). Furthermore, the magnetic flux and induction current can be controlled when this component is exposed to external magnetic field, because the ions pumping is disturbed. Therefore, this improved neuron model is more effective to detect the mode transition and physical field effect on neural activities induced by changeable magnetic field. It is particularly important that a specially imposed influence is necessary and should be set to $\sigma = 1$ for simplicity; otherwise, the discrete m-Rulkov model described in (5) is iterated unbounded. To the best of our knowledge, this is the first time that a discrete neuron model coupled with memristor is proposed for estimating the biophysical effect.

The stability of a discrete map is depicted by its fixed point. The fixed point of the m-Rulkov model satisfies the following:

$$\tilde{x} = F(\tilde{x}, \tilde{y}) + k\tanh(\tilde{\varphi})\tilde{x}, \tilde{y} = \tilde{y} - \mu\tilde{x}, \text{and} \tilde{\varphi} = \tilde{\varphi} + \varepsilon\tilde{x}. \tag{6}$$

Because $\tilde{x} = 0$ and $F(0, \tilde{y}) = \alpha + \tilde{y}$, it can be solved as follows:

$$S = (\tilde{x}, \tilde{y}, \tilde{\varphi}) = (0, -\alpha, \xi) \tag{7}$$

where ξ is an arbitrary value depending on the memristor initial state. Therefore, the m-Rulkov model has infinite fixed points on the φ-axis.

The fixed point can be unstable or stable and its stability can be determined by its Jacobian eigenvalues. The Jacobian of the m-Rulkov model at S is derived as follows:

$$\mathbf{J}_S = \begin{bmatrix} F'(\tilde{x}) + k\tanh(\tilde{\varphi}) & F'(\tilde{y}) & k\text{sech}^2(\tilde{\varphi})\tilde{x} \\ -\mu & 1 & 0 \\ \varepsilon & 0 & 1 \end{bmatrix} \tag{8}$$

where $F'(x)$ and $F'(y)$ are the partial derivatives of the function $F(x, y)$ with respect to x and y, respectively. Substituting (7) into (8), the eigenvalues of the Jacobian in (8) can be calculated by the following:

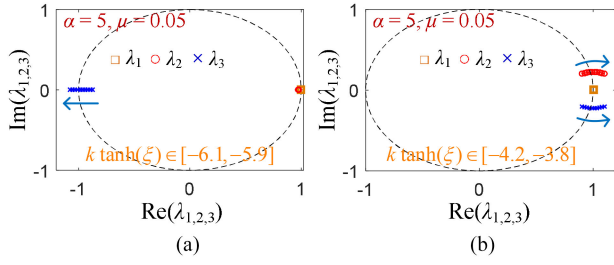$$\lambda_1 = 1, \lambda_{2,3} = b \pm \sqrt{b^2 - c} \tag{9}$$

Fig. 3. For $\alpha = 5$ and $\mu = 0.05$, the loci of three eigenvalues with respect to the memristor parameter. (a) $k\tanh(\xi)$ increasing from -6.1 to -5.9. (b) $k\tanh(\xi)$ increasing from -4.2 to -3.8.
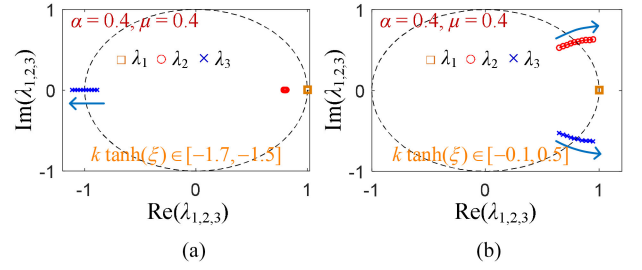

Fig. 4. For $\alpha = 0.4$ and $\mu = 0.4$, the loci of three eigenvalues with respect to the memristor parameter. (a) $k\tanh(\xi)$ increasing from -1.7 to -1.5. (b) $k\tanh(\xi)$ increasing from -0.1 to 0.5.
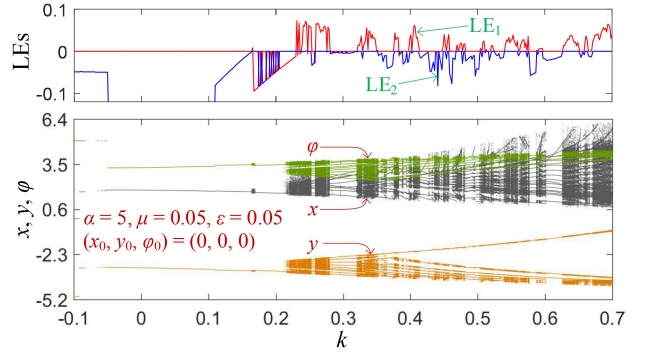
where $b = 0.5(1 + \alpha + k\tanh\xi)$ and $c = \alpha + \mu + k\tanh\xi$. Hence, the eigenvalues are independent of the parameter ε.

Obviously, if $|\lambda_2| > 1$ or $|\lambda_3| > 1$, the fixed point S is unstable; otherwise it is critical stable due to $|\lambda_1| = 1$. When the parameters b and c in (9) are specified, the two eigenvalues λ_2 and λ_3 in (9) can be calculated and the instability of the m-Rulkov model can be determined.

The parameters k and ξ are related to the discrete memristor. To provide a convenience for analysis, we take $k\tanh(\xi)$ as a variable parameter and call it the memristor parameter. In the following, we consider two sets of representative model parameter settings (α and μ) as examples and they are used to generate hyperchaos and bursting firings, respectively.

First, a set of representative model parameters are set to $\alpha = 5$ and $\mu = 0.05$ for bursting firings. The critical stable interval of memristor parameter is solved from (9) as follows:

$$-6.025 \leq k\tanh(\xi) \leq -4.05. \tag{10}$$

Because $|\tanh(\xi)| < 1$, the induction strength should satisfy the condition that $|k| > 4.05$. Otherwise, (10) has no solution.

When the memristor parameter increases within $[-6.1, -5.9]$ and $[-4.2, -3.8]$, we draw the loci of the three eigenvalues in Fig. 3. One can see that λ_1 is always on the unit circle and λ_2, λ_3 are depended on the memristor parameter. When $k\tanh(\xi)$ increases from -6.1 to -5.9, λ_2 is inside the unit circle, whereas λ_3 goes through the unit circle via -1. When $k\tanh(\xi)$ increases from -4.2 to -3.8, λ_2, λ_3 are a pair of conjugate complex roots and they cross the unit circle from the first and fourth quadrants, respectively. From (10) and Fig. 3, we can know that the m-Rulkov model has a period-doubling bifurcation at $k\tanh(\xi) = -6.025$ and a Hopf bifurcation at $k\tanh(\xi) = -4.05$.

Secondly, another set of representative model parameters are set to $\alpha = 0.4$ and $\mu = 0.4$ for hyperchaos. Then the critical stable interval of memristor parameter is solved from (9) as follows:

$$-1.6 \leq k\tanh(\xi) \leq 0.2. \tag{11}$$

Similarly, the induction strength must satisfy the condition $|k| > 0.2$. Otherwise, (11) has no solution.

When the memristor parameter increases within $[-1.7, -1.5]$ and $[-0.1, 0.5]$, the loci of the three eigenvalues are plotted in Fig. 4. Similarly, we can observe from (11) and Fig. 4 that a period-doubling bifurcation occurs at $k\tanh(\xi) = -1.6$ and a Hopf bifurcation appears at $k\tanh(\xi) = 0.2$.

Fig. 5. Induction strength-relied bifurcation diagrams for x, y, φ as well as the first two LE spectra.

Consequently, when the memristor parameter falls in the interval restricted by (10) or (11), the m-Rulkov model is critical stable, otherwise it is unstable. With the change of the memristor parameter, the m-Rulkov model has the routes of period-doubling bifurcation and Hopf bifurcation. Due to $|\lambda_1| = 1$, the memristor parameter-relied stability of the presented model cannot be directly evaluated by (10) or (11), but it can be determined by the numerical results.

III. MAGNETIC INDUCTION-RELIED REGIME TRANSITION

This section studies the magnetic induction-relied regime transition behaviors of the m-Rulkov model with fixed $\alpha = 5$, $\mu = 0.05$, and $\varepsilon = 0.05$, and $(x_0, y_0) = (0, 0)$. The bifurcation diagrams are plotted by measuring the spike value of x per cycle, rather than the sampling value of x per iteration in the traditional sense. Besides, the Lyapunov exponent (LE) spectra are calculated using the Wolf's Jacobian-based algorithm [25].

A. Induction Strength-Relied Regime Transition

The memristor initial state is set as $\varphi_0 = 0$ and the induction strength k is taken as an alterable parameter. The bottom of Fig. 5 displays the bifurcation diagrams for x, y, φ simultaneously, and the top of Fig. 5 plots the first two LEs. As k increases from -0.1, the m-Rulkov model starts with silence and jumps into tonic spiking with zero largest LE at $k = -0.091$. The periodic spiking lasts until $k = 0.230$, during which there is a narrow chaotic spiking interval with positive largest LE at $k \in [0.1640, 0.1657]$. Thereafter, the m-Rulkov model goes into
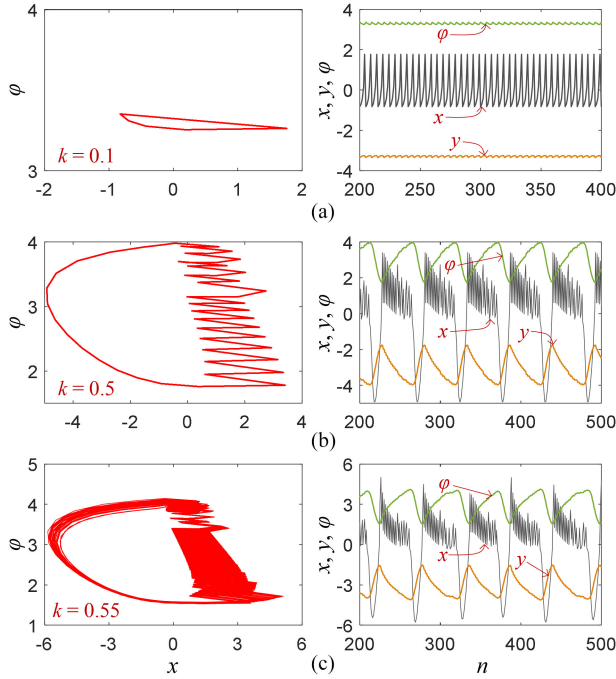
Fig. 6. Induction strength-relied phase diagrams in the $x - \varphi$ plane (left) and firing patterns for x, y, φ (right). (a) Tonic spiking at $k = 0.1$. (b) Periodic bursting at $k = 0.5$. (c) Chaotic bursting at $k = 0.55$.

the interval where periodic bursting and chaotic bursting appear alternately, and finally settles into chaotic bursting. As can be found, with the change of k, the model (5) simulates essential regimes of neuronal firing patterns, such as the silence, tonic spiking, periodic bursting, and chaotic bursting [29].

Corresponding to the induction strength-relied bifurcation scenarios in Fig. 5, three representative values of the induction strength k are determined for the m-Rulkov model. Fig. 6 depicts three sets of phase diagrams in the $x - \varphi$ plane (left) and firing patterns for x, y, φ (right). As can be observed, Fig. 6(a) displays a tonic spiking regime, Fig. 6(b) exhibits a periodic bursting regime, and Fig. 6(c) shows a chaotic bursting regime. For the spiking regimes, the increase of k leads to the decrease of the interspike intervals; whereas for the bursting regimes, the increase of k results in the increase of the spike number per burst. In addition, the chaotic bursting regimes with different irregular spikes easily appear in the m-Rulkov model and they cannot be found in the original Rulkov model. These results manifest that the memristor magnetic induction can cause complex regime transition behaviors in the m-Rulkov model.

B. Memristor Initial State-Relied Regime Transition

The induction strength k is fixed as $k = 0.5$, and the memristor initial state φ_0 is treated as an alterable parameter. The bottom of Fig. 7 depicts the bifurcation diagrams for x, y, φ simultaneously, and the top of Fig. 7 plots the first two finite-time LEs. The dynamical behaviors exhibited in the bifurcation diagrams and finite-time LEs are basically consistent, but have difference in the vicinity of $\varphi_0 = 3$ due to transient chaos. When φ_0 increases from -6, the m-Rulkov model begins with silence and mutates
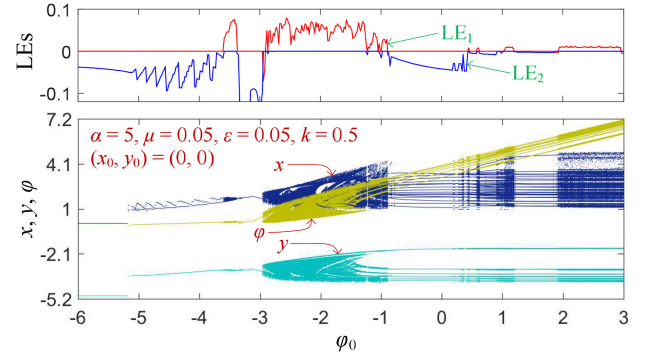

Fig. 7. Memristor initial state-relied bifurcation diagrams for x, y, φ along with the first two LE spectra.
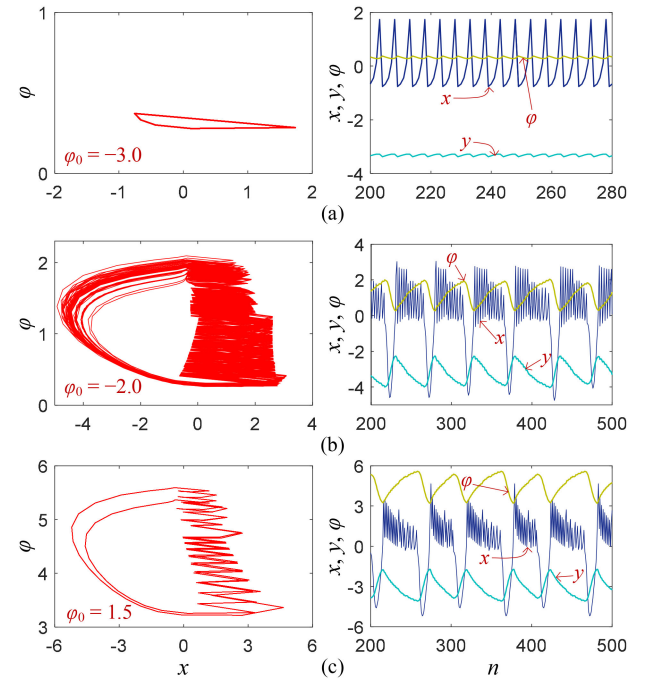

Fig. 8. Memristor initial state-relied phase diagrams in the $x - \varphi$ plane (left) and firing patterns for x, y, φ (right). (a) Tonic spiking at $\varphi_0 = -3.0$. (b) Chaotic bursting at $\varphi_0 = -2.0$. (c) Periodic bursting at $\varphi_0 = 1.5$.

into tonic spiking at $\varphi_0 = -5.185$. The periodic spiking lasts until $\varphi_0 = -2.944$, during which there is a narrow chaotic spiking interval at $\varphi_0 \in [-3.598, -3.378]$. Afterwards, the model (5) enters into the interval where periodic bursting and chaotic bursting appear alternately, and finally settles into the chaotic bursting. Thus, with the change of the memristor initial state φ_0, the model (5) can simulate the essential regimes of neuronal firing patterns as well. Therefore, the bifurcation scenarios in both the Figs. 5 and 7 have complex regime transition behaviors.

Similarly, from the bifurcation scenarios in Fig. 7, three representative values of the memristor initial state φ_0 are selected. Fig. 8 shows three sets of phase diagrams in the $x - \varphi$ plane (left) and firing patterns for x, y, φ (right). Concretely, Fig. 8(a) reveals a tonic spiking regime, Fig. 8(b) claims a chaotic bursting regime with irregular spikes, and Fig. 8(c) exhibits a periodic bursting regime with double bursters. For the spiking regimes,
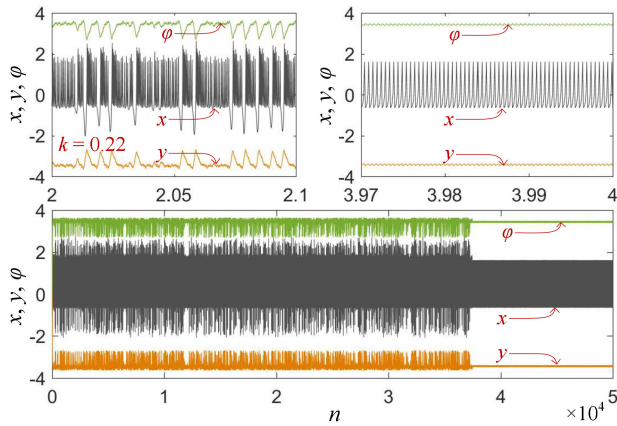
Fig. 9. Iterative sequences of transient chaotic bursting with steady periodic spiking at $k = 0.22$ ($\varphi_0 = 0$), where the transient chaotic bursting motion changes to a steady-state periodic spiking motion at $n = 3.75 \times 10^4$. The two images above are partial enlargements of the image below.
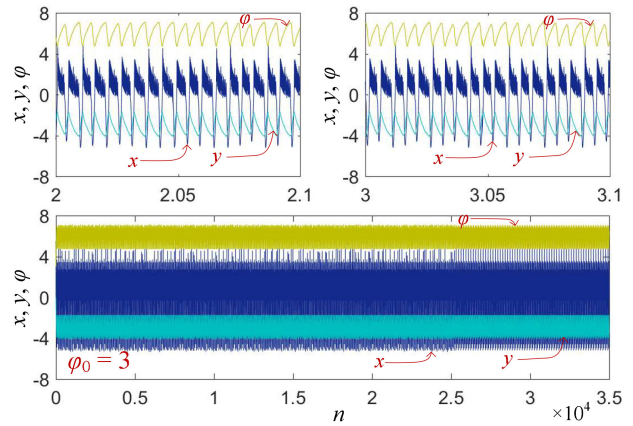

Fig. 10. Iterative sequences of transient chaotic bursting with steady periodic bursting at $\varphi_0 = 3.0$ ($k = 0.5$), where the transient chaotic bursting motion changes to a steady-state periodic bursting motion at $n = 2.53 \times 10^4$. The two images above are partial enlargements of the image below.

the increase of φ_0 causes the decrease of the interspike intervals. While for the chaotic and periodic bursting regimes, the increase of φ_0 keeps the interburst intervals basically unchanged. The results declare that the memristor initial state can also cause complex regime transition behaviors in the m-Rulkov model. Namely, the infinitely many attractors with extreme multistability are coexisted in the m-Rulkov model [4].

C. Transient Chaotic Bursting Regimes

Transient chaos is usually accompanied with boundary crisis that can show intermittent behavior. A system trajectory behaves chaotically on finite-time intervals and then passes to a steady nonchaotic state that can be periodic or stationary as well. The phenomenon of transient chaos can often occur in many chaotic systems [31].

From Fig. 5, one can find that the dynamical behaviors represented by the LE spectra and bifurcation diagrams are inconsistent within some special intervals of k due to the appearance of transient chaos. For instance, when $k = 0.22$, the largest LE shown in the top of Fig. 5 equals to zero, while the bifurcation behavior given in the bottom of Fig. 5 is chaotic bursting regime. Fig. 9 displays the corresponding iterative sequences of the transient chaotic bursting with steady periodic spiking in iterative interval $[1, 5 \times 10^4]$. The relatively long transient chaotic motion occurs at the beginning and changes to a steady-state periodic motion at $n = 3.75 \times 10^4$. The sequence in $[2 \times 10^4, 2.1 \times 10^4]$ is chaotic bursting, while that in $[3.97 \times 10^4, 4 \times 10^4]$ is periodic spiking. This result indicates that the m-Rulkov model has a regime transition from the long-term transient chaotic bursting to final steady periodic spiking.

Another interesting instance can be seen in Fig. 7. When $\varphi_0 = 3.0$, the largest LE depicted in the top of Fig. 7 is zero, while the bifurcation behavior drawn in the bottom of Fig. 7 is chaotic. Fig. 10 shows the corresponding iterative sequences of transient chaotic bursting with steady periodic bursting in iterative interval $[1, 3.5 \times 10^4]$. A long transient chaotic bursting motion appears

in the starting interval and then goes to a steady-state periodic bursting motion at $n = 2.53 \times 10^4$. As shown in Fig. 10, the iterative sequence in $[2 \times 10^4, 2.1 \times 10^4]$ is chaotic bursting with irregular bursters, while that in $[3.97 \times 10^4, 4 \times 10^4]$ is periodic bursting with triple bursters. The result shown here is distinguishing from that shown in Fig. 9 and means that the m-Rulkov model has a regime transition from the transient chaotic bursting to steady periodic bursting.

In summary, when introducing the memristive magnetic induction, the m-Rulkov model can produce biologically plausible and significant magnetic induction-relied regime transition behaviors. Then, the actual firing activities in biological neurons can be better characterized when biophysical memory effect is supplied.

IV. HYPERCHAOTIC FIRING BEHAVIORS AND ATTRACTORS

To further demonstrate complex dynamics of the m-Rulkov model, we explore its memristor-related hyperchaotic firing behaviors in aspects of mixed bifurcation plot and phase trajectory. The parameter and initial state settings are changed as $\alpha = 0.4$, $\mu = 0.4$, and $\varepsilon = 1$, and $(x_0, y_0) = (0, 0)$.

A. Memristor-Related Hyperchaotic Firing Behaviors

A mixed bifurcation plot is depicted in the $\varphi_0 - k$ plane by measuring the spike value of iterative sequence per cycle and its first two finite-time LEs [27]. Fig. 11 shows the mixed bifurcation plot of the m-Rulkov model for $\varphi_0 \in [-2, 2]$ and $k \in [-2, 2]$. The red area labeled by HC represents hyperchaos, the pink area by CH represents chaos, the khaki area by QP represents the quasi-period, the purple area by MP represents the multiple period with a cycle number of more than 8, the black area by UB represents the unbounded behavior, and the rest areas labeled by P1 to P7 represent period-1 to period-7, respectively. Note that the hyerchaotic and quasi-periodic firing behaviors need to be proved by the collaboration of the finite-time LEs. Therefore, the mixed bifurcation plotted in Fig. 11 can exhibit
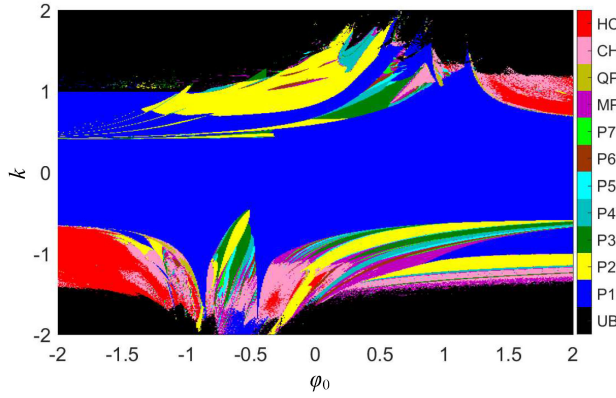
Fig. 11. Complex hyperchaotic firing behaviors depicted by the mixed bifurcation plot in the $\varphi_0 - k$ plane under the parameter and initial state settings $\alpha = 0.4$, $\mu = 0.4$, and $\varepsilon = 1$, and $(x_0, y_0) = (0, 0)$.
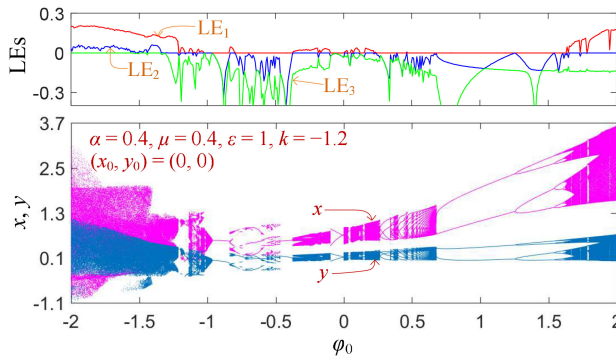

Fig. 12. Memristor initial state-relied bifurcation diagrams for x, y along with the LE spectra, where $\alpha = 0.4$, $\mu = 0.4$, $\varepsilon = 1$, $k = -1.2$, and $(x_0, y_0) = (0, 0)$.

complex hyperchaotic firing behaviors that are extremely related to the induction strength and memristor initial state.

To intuitively display how the bifurcation routes to chaos, we draw the bifurcation plots with the change of φ_0 by fixing $k = -1.2$. The bottom of Fig. 12 shows the bifurcation diagrams for variables x and y, and the top of Fig. 12 gives the corresponding finite-time LEs. Note that we do not give the bifurcation diagram of variable φ for easy observation. As the memristor initial state φ_0 increases from -2, the motion orbits of the m-Rulkov model first show hyperchaotic firing patterns with two positive LEs, and then display chaotic firing patterns with one positive LE at $\varphi_0 = -1.33$, and finally behave quasi-periodic firing patterns with two zero LEs at $\varphi_0 = -1.01$. So there is a specific quasi-periodic bifurcation route to chaos around $\varphi_0 = -1.01$. When φ_0 varies within the interval $[-0.97, -0.37]$, the motion orbits exhibit periodic firing patterns with negative largest LE, but also display chaotic firing patterns in the narrowly sandwiched interval $[-0.84, -0.80]$. When $\varphi_0 \in [-0.37, 0.24]$, the motion orbits oscillate in chaotic firing patterns with some periodic windows due to crisis scenarios. When $\varphi_0 \in [0.24, 0.68]$, the motion orbits are in multi-periodic firing patterns. Afterwards, when φ_0 increases within the interval $[0.68, 2]$, the motion orbits have dynamical transitions from period-2, to period-4, to period-8, further to period-16, and finally to chaos
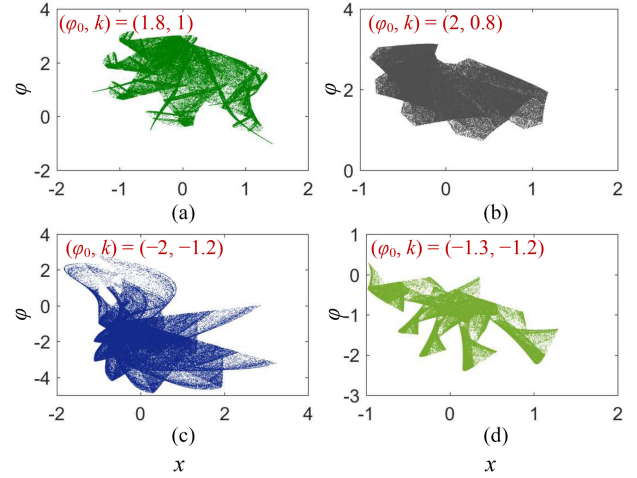

Fig. 13. Phase trajectories for four sets of memristor parameters. (a) Chaotic attractor for $(\varphi_0, k) = (1.8, 1)$. (b) Hyperchaotic attractor for $(\varphi_0, k) = (2, 0.8)$. (c) Hyperchaotic attractor for $(\varphi_0, k) = (-2, -1.2)$. (d) Chaotic attractor for $(\varphi_0, k) = (-1.3, -1.2)$.

TABLE I
PERFORMANCE INDICATORS FOR FOUR SETS OF ITERATIVE SEQUENCES

(φ_0, k)	(LE$_1$, LE$_2$)	SE	PE	CorDim
$(1.8, 1)$	$(0.1304, 0.0001)$	0.9232	4.2881	1.4525
$(2, 0.8)$	$(0.0789, 0.0620)$	0.9044	3.5220	1.8641
$(-2, -1.2)$	$(0.1968, 0.0303)$	0.8772	4.4975	1.6426
$(-1.3, -1.2)$	$(0.1216, 0.0000)$	0.8785	3.1965	1.7012

due to the period-doubling bifurcation route to chaos. Therefore, the m-Rulkov model has complex bifurcation dynamics and its firing patterns are extremely relied on its memristor initial state, indicating the emergence of extreme multistability [4].

B. Hyperchaotic and Chaotic Attractors

Four representative sets of memristor parameters are picked from the red and pink areas in Fig. 11, namely $(\varphi_0, k) = (1.8, 1)$, $(2, 0.8)$, $(-2, -1.2)$, and $(-1.3, -1.2)$, respectively. For the m-Rulkov model, the phase trajectories projected on the $x - \varphi$ plane are obtained and shown in Fig. 13. Two hyperchaotic attractors and two chaotic attractors are demonstrated. Obviously, all these hyperchaotic and chaotic attractors have fantastic fractal structures.

Besides, we also evaluate these sequences using different performance indicators, which include the first two finite-time LEs (LE$_1$, LE$_2$), spectral entropy (SE), permutation entropy (PE), and correlation dimension (CorDim) [25]. The length of sequences for the first two LEs is determined as 5×10^5 and that for other performance indicators is set to 10^5. The test results of the generated sequences under the four sets of memristor parameters are listed in Table I. As seen that, the sequences under $(\varphi_0, k) = (2, 0.8)$, $(-2, -1.2)$ have two positive LEs, representing hyperchaos; whereas those under $(\varphi_0, k) = (1.8, 1)$, $(-1.3, -1.2)$ have only one positive LE, representing chaos.

However, they all have large test values, indicating excellent performance indicators. This implies that the introduced memristor can significantly enhance the chaos complexity of the original Rulkov model. Therefore, the m-Rulkov model has the same properties with other discrete chaotic maps and can also be applied to various industrial fields.

C. Random Number Generator

Random numbers are widely applied in many industrial fields [32], [33]. Since the m-Rulkov model can generate the chaotic sequences with excellent performance indicators, it can achieve good performance in this application. Here, we design random number generators using the four sets of chaotic sequences, which are produced by the m-Rulkov model under the four sets of memristor parameters listed in Table I.

Suppose a chaotic sequence generated by the m-Rulkov model is $S = \{s_1, s_2, \ldots, s_n, \ldots\}$. Then random numbers are produced by the following:

$$P_i = B(s_n)_{41:48} \qquad (12)$$

where $B(\cdot)$ is to transform a value to be a 52-bit float number obeying the IEEE float-point standard. Thus, eight binary numbers are produced for each output of the chaotic sequence.

The random numbers are expected to have high randomness. The NIST SP800-22 [34] is used to test the random numbers. It is a convinced and all-side test standard that contains 15 subtests. Each subtest aims to find the nonrandom area in a random number sequence. A significance level is used in the test suite. According to the settings and requirements in [34], we set the significance level as 0.01, and the length of binary sequence as 10^6. Then, a total number of 120 binary sequences are generated and tested.

In our experiments, we first generate a chaotic sequence $\{x_1, x_2, \ldots, x_n, \ldots\}$ with length 120×125000, and then produce 120 binary sequences with 10^6 bits. The pass rate larger than 0.9628 is considered to pass the related sub-test [34]. Table II lists the test results of the four sets of chaotic sequences generated by the m-Rulkov model. One can see that they can pass all the subtests of the NIST SP800-22 test suite. This means that the m-Rulkov model has complex chaotic dynamics and can produce random numbers with high randomness.

D. Performance Comparisons

To compare the performance of the presented 3-D m-Rulkov model with several existing discrete and continuous neuron models in generating random numbers, we select the m-Rulkov model under the memristor parameters $(\varphi_0, k) = (2, 0.8)$ and four existing discrete and continuous neuron models with their typical parameter settings as the chaotic sequence sources in (12) to generate random numbers. These existing neuron models include the 2-D discrete Rulkov model (2-D Rulkov1 model) [26], 2-D discrete Rulkov model based on continuous nonlinearity (2-D Rulkov2 model) [35], 3-D memristor-based continuous HR model (3-D mHR model) [5], and 3-D continuous Morris-Lecar model (3-D M-L model) [36]. Note that these existing neuron models are initiated from their origin.

TABLE II
NIST SP800-22 TEST RESULTS FOR FOUR SETS OF RANDOM NUMBERS GENERATED BY THE M-RULKOV MODEL

No.	Sub-tests	(φ_0, k)			
		(1.8, 1)	(2, 0.8)	(−2, −1.2)	(−1.3, −1.2)
01	Frequency	0.9750	1.0000	0.9750	0.9917
02	Block Frequency	1.0000	0.9917	0.9750	0.9833
03	Cum. Sums* (F)	0.9833	1.0000	0.9833	0.9917
	Cum. Sums* (R)	0.9667	1.0000	0.9833	0.9917
04	Runs	0.9917	1.0000	0.9833	0.9750
05	Longest Runs	0.9833	1.0000	0.9667	0.9917
06	Rank	0.9833	1.0000	1.0000	0.9917
07	FFT	0.9917	1.0000	0.9750	1.0000
08	Non-Ovla. Temp.*	0.9896	0.9917	0.9889	0.9912
09	Ovla. Temp.	1.0000	1.0000	0.9667	0.9833
10	Universal	0.9667	1.0000	0.9917	0.9917
11	Appr. Entropy	0.9833	0.9917	1.0000	0.9833
12	Ran. Exc.*	0.9850	0.9923	0.9865	0.9891
13	Ran. Exc. Var.*	0.9896	0.9877	0.9842	0.9757
14	Serial (1st)	0.9917	1.0000	1.0000	1.0000
	Serial (2nd)	0.9833	1.0000	1.0000	0.9917
15	Linear complexity	0.9750	0.9917	1.0000	1.0000
	Success No.	15/15	15/15	15/15	15/15

Note: *Non-Ovla. Temp., Ran. Exc., and Ran. Exc. Var. tests are comprised of 148, 8, and 18 subtests, respectively.

TABLE III
PERFORMANCE COMPARISONS FOR THE CHAOTIC SEQUENCES GENERATED BY SOME DISCRETE AND CONTINUOUS NEURON MODELS

Neuron Models	Typical Settings	InfoEn	SE*	PE*
3D m-Rulkov model	$(\varphi_0, k) = (2, 0.8)$	7.7545	0.9044	3.5220
2D Rulkov1 model [26]	$(\alpha, \sigma) = (4.5, 0.14)$	4.8350	0.8325	1.4678
2D Rulkov2 model [35]	$(\alpha, \sigma) = (4.5, 0.001)$	6.3827	0.9107	2.6541
3D mHR model [5]	$m = 1$	7.4287	0.4650	0.7091
3D M-L model [36]	$(V_K, \varepsilon) = (-410, 0.1)$	6.9753	0.4559	0.7625
3D M-L model [36]	$(V_K, \varepsilon) = (-500, 0.1)$	7.1233	0.3499	0.7781

Note: *The SE and PE measurements are based on the chaotic sequences directly generated by the above neuron models.

Afterward, we use information entropy (InfoEn) to compute the randomness of the generated random numbers. The InfoEn of a sequence S can be computed by the following:

$$H(S) = -\sum_{j=1}^{2^n} p(S_j) \log_2 p(S_j) \qquad (13)$$

where S_j is the jth possible value in S, $p(S_j)$ is the probability of S_j, and n is the bit length in each value. In our measurement, each 8 bits of random numbers are set as a unit and the maximum value of InfoEn is thereby obtained as 8. A larger InfoEn value implies the higher randomness of the random numbers generated by the neuron model.

Table III lists the InfoEn values of different random numbers with 10^5-bit length generated by different neuron models under their typical parameter settings. As can be observed, the random numbers generated using the 3-D m-Rulkov model have larger
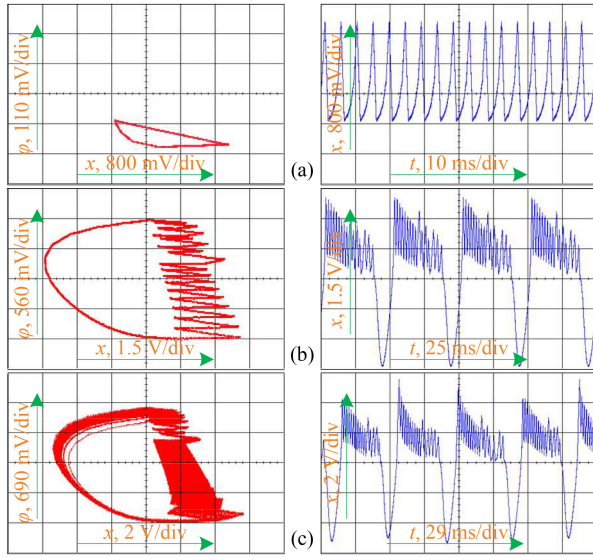
Fig. 14. Measured induction strength-relied phase diagrams in the $x - \varphi$ plane (left) and iterative sequences of variable x (right). (a) Tonic spiking at $k = 0.1$. (b) Periodic bursting at $k = 0.5$. (c) Chaotic bursting at $k = 0.55$.

Fig. 15. Measured memristor initial state-relied phase diagrams in the $x - \varphi$ plane (left) and time sequences of variable x (right). (a) Tonic spiking at $\varphi_0 = -3.0$. (b) Chaotic bursting at $\varphi_0 = -2.0$. (c) Periodic bursting at $\varphi_0 = 1.5$.

InfoEn values than that using the existing discrete and continuous neuron models. When random numbers are used in many applications, they are expected to have high randomness. Thus, the random numbers generated by the 3-D m-Rulkov model are suitable for many engineering applications.

Moreover, Table III lists the SE and PE of the 10^5-bit length sequences directly generated by different neuron models. One can observe that the 3-D m-Rulkov model possesses relatively larger PE than all the existing discrete and continuous neuron models, and the discrete neuron models can achieve larger SE than the existing constinuous neuron models. The comparative results signify that the chaotic sequences generated by the m-Rulkov model have more complex chaotic dynamics.

V. HARDWARE EXPERIMENTAL VERIFICATION

The on-chip digital devices can be used to implement numerous neuron models. In this section, we elaborate a hardware platform for implementing the m-Rulkov model based on a 32-bit microcontroller and then acquire diverse spiking-bursting sequences in physical. Due to the properties of pony-size, low-cost, and ultralow power, the microcontroller is widely applied in industrial electronics [32].

The programmable hardware platform mainly contains a 32-bit STM32F407 microcontroller, two 12-bit TLV5618 digital-to-analog converters, and a voltage transfer circuit. The microcontroller is used for digitally implementing the m-Rulkov model, the digital-to-analog converters output analog voltage sequences, and the voltage transfer circuit realizes the unipolar-to-bipolar voltage conversion. The executable program of the m-Rulkov model in (5) is coded using C language and downloaded to the 32-bit microcontroller. All the parameter and initial settings are preloaded to the programmable hardware platform. When switching on the power supply, the analog voltage
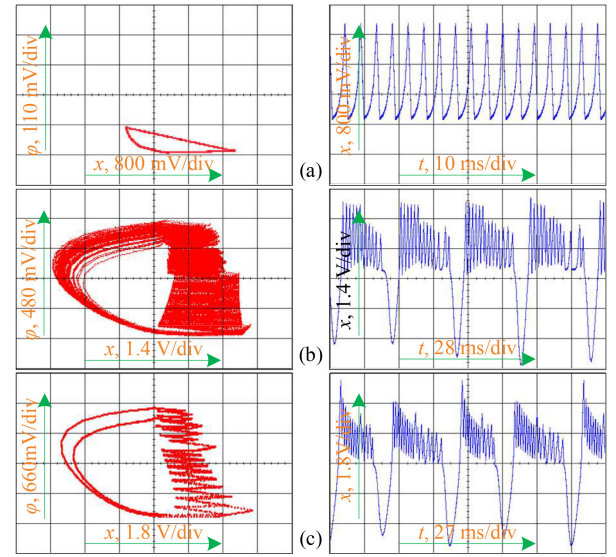
sequences or phase diagrams in the XY mode can be captured by a digital oscilloscope.

First, the parameter and initial state settings are fixed as $\alpha = 5$, $\mu = 0.05$, and $\varepsilon = 0.05$, and $(x_0, y_0, \varphi_0) = (0, 0, 0)$. Following the numerical results in Fig. 6, three concerned values of the induction strength k are determined for the m-Rulkov model. The induction strength-relied phase diagrams in the $x - \varphi$ plane and time sequences of variable x are experimentally measured by the digital oscilloscope, as shown in Fig. 14. Second, the parameter and initial state settings are fixed as $\alpha = 5$, $\mu = 0.05$, $\varepsilon = 0.05$, and $k = 0.5$, and $(x_0, y_0) = (0, 0)$. According to the numerical results given in Fig. 8, three concerned values of the memristor initial state φ_0 are selected for the m-Rulkov model. The memristor initial state-relied phase diagrams in the $x - \varphi$ plane and time sequences of variable x are experimentally measured by the digital oscilloscope, as shown in Fig. 15. The experimental results in Figs. 14 and 15 perfectly validate the simulation results in Figs. 6 and 8. This manifests the feasibility of the hardware platform for the presented m-Rulkov model.

VI. CONCLUSION

Magnetic flux can estimate the contributions of the magnetic field induced by current and running charges, and the involvement of flux-controlled memristor can describe synaptic plasticity and controllability of synapse under external field. The inner ions pumping is stochastic and paroxysmal in the cell, and the induced magnetic field is changeable, while the magnetic flux is a kind of statistical scalar and the transient effect is missed when the continuous model is applied. Besides, the biological neurons show rapid mode transition under external stimulus. Therefore, the combination of discrete memristor and map is reliable to estimate the biophysical effect in neurons and nervous system.

With this knowledge, this article first constructed a discrete memristor and then presented an m-Rulkov neuron model by involving the discrete memristor. The m-Rulkov model has infinite fixed points and its stability depends strongly on the control parameters and memristor initial state. The bifurcation routes of the m-Rulkov model were declared by detecting the eigenvalue loci and its complex spiking-bursting transitions, transient chaotic bursting, and hyperchaotic firing behaviors were investigated using numerical measures. The results showed that the memristor can be used to simulate the magnetic induction and its dynamical effects on the m-Rulkov model can be effectively revealed. In brief, the presented m-Rulkov model produces biologically plausible and significant magnetic induction-relied regime transition behaviors, which can well characterize the actual firing activities in biological neurons. In addition, compared with continuous neuron models, the m-Rulkov model has lower dimensions for generating hyperchaotic behaviors and can produce random numbers with higher randomness. However, how to explain the complex kinetics mechanism of these regime transition behaviors theoretically remains to be further studied.

REFERENCES

[1] R. M. Rose and J. L. Hindmarsh, "The assembly of ionic currents in a thalamic neuron i. The three-dimensional model," *Proc. Roy. Soc. London B, Biol. Sci.*, vol. 237, no. 1288, pp. 267–288, Aug. 1989.

[2] K. Eshraghian *et al.*, "Memristive device fundamentals and modeling: Applications to circuits and systems simulation," *Proc. IEEE*, vol. 100, no. 6, pp. 1991–2007, Jun. 2012.

[3] F. Corinto and M. Forti, "Memristor circuits: Bifurcations without parameters," *IEEE Trans. Circuits Syst. I, Reg. Papers*, vol. 64, no. 6, pp. 1540−1551, Jun. 2017.

[4] M. Chen, M. Sun, H. Bao, Y. Hu, and B. Bao, "Flux-charge analysis of two-memristor-based Chua's circuit: Dimensionality decreasing model for detecting extreme multistability," *IEEE Trans. Ind. Electron.*, vol. 67, no. 3, pp. 2197–2206, Mar. 2020.

[5] H. Bao, A. Hu, W. Liu, and B. Bao, "Hidden bursting firings and bifurcation mechanisms in memristive neuron model with threshold electromagnetic induction," *IEEE Trans. Neural Netw. Learn. Syst.*, vol. 31, no. 2, pp. 502–511, Feb. 2020.

[6] Q. Hong, L. Zhao, and X. Wang, "Novel circuit designs of memristor synapse and neuron," *Neurocomputing*, vol. 330, pp. 11–16, Feb. 2019.

[7] A. L. Hodgkin and A. F. Huxley, "A quantitative description of membrane current and its application to conduction and excitation in nerve," *J. Physiol.*, vol. 117, no. 4, pp. 500–544, Aug. 1952.

[8] R. Behdad, S. Binczak, A. S. Dmitrichev, V. I. Nekorkin, and J. M. Bilbault, "Artificial electrical Morris-Lecar neuron," *IEEE Trans. Neural Netw. Learn. Syst.*, vol. 26, no. 9, pp. 1875–1884, Sep. 2015.

[9] L. Chua, "If it's pinched it's a memristor," *Semicond. Sci. Technol.*, vol. 29, no. 10, Sep. 2014, Art. no. 104001.

[10] V. Rajamani, H. Kim, and L. Chua, "Morris-Lecar model of third-order barnacle muscle fiber is made of volatile memristors," *Sci. China Inf. Sci.*, vol. 61, no. 6, Jun. 2018, Art. no. 060426.

[11] P. Yao *et al.*, "Fully hardware-implemented memristor convolutional neural network," *Nature*, vol. 577, no. 7550, pp. 641–646, Jan. 2020.

[12] S. Kumar, J. P. Strachan, and R. S. Williams, "Chaotic dynamics in nanoscale NbO_2 Mott memristor for analogue computing," *Nature*, vol. 548, no. 7667, pp. 318–321, Aug. 2017.

[13] V. K. Sangwan *et al.*, "Multi-terminal memtransistors from polycrystalline monolayer molybdenum disulfide," *Nature*, vol. 554, no. 25747, pp. 500–504, Feb. 2018.

[14] T. Fu *et al.*, "Bioinspired bio-voltage memristors," *Nat. Commun.*, vol. 11, Apr. 2020, Art. no. 1861.

[15] S. Kumar, R. S. Williams, and Z. Wang, "Third-order nanocircuit elements for neuromorphic engineering," *Nature*, vol. 585, no. 3474, pp. 518–523, Sep. 2020.

[16] Q. Hong, H. Chen, J. Sun, and C. Wang, "Memristive circuit implementation of a self-repairing network based on biological astrocytes in robot application," *IEEE Trans. Neural Netw. Learn. Syst.*, to be published, doi: 10.1109/TNNLS.2020.3041624.

[17] E. Bilotta, P. Pantano, and S. Vena, "Speeding up cellular neural network processing ability by embodying memristors," *IEEE Trans. Neural Netw. Learn. Syst.*, vol. 28, no. 5, pp. 1228–1232, May 2017.

[18] Z. I. Mannan, S. P. Adhikari, C. Yang, R. K. Budhathoki, H. Kim, and L. Chua, "Memristive imitation of synaptic transmission and plasticity," *IEEE Trans. Neural Netw. Learn. Syst.*, vol. 30, no. 11, pp. 3458–3470, Nov. 2019.

[19] M. Lv, C. Wang, G. Ren, and J. Ma, "Model of electrical activity in a neuron under magnetic flow effect," *Nonlinear Dyn.*, vol. 85, no. 3, pp. 1479–1490, Apr. 2016.

[20] J. Ma and J. Tang, "A review for dynamics in neuron and neuronal network," *Nonlinear Dyn.*, vol. 89, no. 3, pp. 1569–1578, Aug. 2017.

[21] Y. Xu, Y. Jia, M. Ge, L. Lu, L. Yang, and X. Zhan, "Effects of ion channel blocks on electrical activity of stochastic Hodgkin-Huxley neural network under electromagnetic induction," *Neurocomputing*, vol. 283, pp. 196–204, Mar. 2018.

[22] M. Ge, Y. Jia, Y. Xu, and L. Yang, "Mode transition in electrical activities of neuron driven by high and low frequency stimulus in the presence of electromagnetic induction and radiation," *Nonlinear Dyn.*, vol. 91, no. 1, pp. 515–523, Jan. 2018.

[23] H. Bao, Y. Zhang, W. Liu, and B. Bao, "Memristor synapse-coupled memristive neuron network: Synchronization transition and occurrence of chimera," *Nonlinear Dyn.*, vol. 100, no. 1, pp. 937–950, Mar. 2020.

[24] B. Bao, H. Li, H. Wu, X. Zhang, and M. Chen, "Hyperchaos in a second-order discrete memristor-based map model," *Electron. Lett.*, vol. 56, no. 15, pp. 769–770, Jul. 2020.

[25] H. Li, Z. Hua, H. Bao, L. Zhu, M. Chen, and B. Bao, "Two-dimensional memristive hyperchaotic maps and application in secure communication," *IEEE Trans. Ind. Electron.*, to be published, doi: 10.1109/TIE.2020.3022539.

[26] N. F. Rulkov, "Modeling of spiking-bursting neural behavior using two-dimensional map," *Phys. Rev. E*, vol. 65, no. 4, Apr. 2002, Art. no. 041922.

[27] H. Bao, Z. Hua, N. Wang, L. Zhu, M. Chen, and B. Bao, "Initials-boosted coexisting chaos in a 2D sine map and its hardware implementation," *IEEE Trans. Ind. Informat.*, vol. 17, no. 2, pp. 1132–1140, Feb. 2021.

[28] K. Pakdaman, "Periodically forced leaky integrate-and-fire model," *Phys. Rev. E*, vol. 63, no. 4, Mar. 2001, Art. no. 041907.

[29] I. Bashkirtseva, V. Nasyrova, and L. Ryashko, "Stochastic spiking- bursting excitability and transition to chaos in a discrete-time neuron model," *Int. J. Bifurcation Chaos*, vol. 30, no. 10, Aug. 2020, Art. no. 2050153.

[30] Z. Hua, B. Zhou, and Y. Zhou, "Sine-transform-based chaotic system with FPGA implementation," *IEEE Trans. Ind. Electron.*, vol. 65, no. 3, pp. 2557–2566, Mar. 2018.

[31] M. F. Danca and N. Kuznetsov, "Hidden chaotic sets in a hopfield neural system," *Chaos Solitons Fractals*, vol. 103, pp. 144–150, Oct. 2017.

[32] M. Bakiri, C. Guyeux, J. F. Couchot, L. Marangio, and S. Galatolo, "A hardware and secure pseudorandom generator for constrained devices," *IEEE Trans. Ind. Informat.*, vol. 14, no. 8, pp. 3754–3765, Aug. 2018.

[33] H. Lin *et al.*, "An extremely simple multi-wing chaotic system: Dynamics analysis, encryption application and hardware implementation," *IEEE Trans. Ind. Electron.*, to be published, doi: 10.1109/TIE.2020.3047012.

[34] A. L. Rukhin *et al.*, "A statistical test suite for random and pseudorandom number generators for cryptographic applications," Nat. Inst. Standard Technol., NIST Special Pub. 800-22, Rev. 1a, Gaithersburg, MD, USA, 2010.

[35] N. F. Rulkov, "Regularization of synchronized chaotic bursts," *Phys. Rev. Lett.*, vol. 86, no. 1, pp. 183−186, Jan. 2001.

[36] B. Bao *et al.*, "Chaotic bursting dynamics and coexisting multi-stable firing patterns in 3D autonomous Morris-Lecar model and microcontroller-based validations," *Int. J. Bifurcation Chaos*, vol. 29, no. 10, Oct. 2019, Art. no. 1950134.

Kexin Li received the B.S. degree in automation in 2020 from Changzhou University, Changzhou, China, where she is currently working toward the M.S. degree in electronics science and technology with the School of Microelectronics and Control Engineering.

Her research interests include discrete nonlinear chaotic systems and discrete memristive neuron model.

Han Bao received the B.S. degree in landscape design from the Jiangxi University of Finance and Economics, Nanchang, China, in 2015, and the M.S. degree in art and design from Changzhou University, Changzhou, China, in 2018. He is currently working toward the Ph.D. degree in nonlinear system analysis and measurement technology with the Nanjing University of Aeronautics and Astronautics, Nanjing, China.

In 2019, he visited the Computer Science Department, The University of Auckland, New Zealand. His research interests include memristive neuromorphic circuit, nonlinear circuits and systems, and artificial intelligence.

Zhongyun Hua (Member, IEEE) received the B.S. degree from Chongqing University, Chongqing, China, in 2011, and the M.S. and Ph.D. degrees from the University of Macau, Macau, China, in 2013 and 2016, respectively, all in software engineering.

He is currently an Associate Professor with the School of Computer Science and Technology, Harbin Institute of Technology, Shenzhen, Shenzhen, China. His research interests include chaotic system, chaos-based applications, multimedia security, and data hiding.

Houzhen Li (Graduate Student Member, IEEE) received the B.S. degree in optoelectronic information science and engineering from the Changshu Institute of Technology, Suzhou, China, in 2019. He is currently working toward the M.S. degree in electronics science and technology with the School of Microelectronics and Control Engineering, Changzhou University, Changzhou, China.

His research interests include memristive neuromorphic circuit and nonlinear circuits and systems.

Bocheng Bao (Member, IEEE) received the B.S. and M.S. degrees in electronic engineering from the University of Electronics Science and Technology of China, Chengdu, China, in 1986 and 1989, respectively, and the Ph.D. degree in information and communication engineering, from the Nanjing University of Science and Technology, Nanjing, China, in 2010.

From 2008 to 2011, he was a Professor with the School of Electrical and Information Engineering, Jiangsu University of Technology, Changzhou, China. He was a Professor with the School of Microelectronics and Control Engineering, Changzhou University, Changzhou. In 2013, he visited the Department of Electrical and Computer Engineering, University of Calgary, Calgary, AB, Canada. His research interests include neuromorphic circuits, power electronic circuits, and nonlinear circuits and systems.

Dr. Bao was a recipient of the IET Premium Award in 2018 and selected as the Highly Cited Researcher 2020 in Cross-Field.

Jun Ma received the graduate degree in physics from Xianyang Normal University, Xianyang, China, in 1996, the M.S. degree in theoretical physics from Guangxi Normal University, Guilin, China, in 2003, and the Ph.D. degree in theoretical physics from Huazhong Normal University, Wuhan, China, in 2010.

He is currently a Professor with the Department of Physics, Lanzhou University of Technology, Lanzhou, China. His research interests include nonlinear control, adaptive control, synchronization, and network of neurons and pattern selection.

Dr. Ma has been an active Associate Editor for *Nonlinear Dynamics* since 2015.